

SUPPLEMENTARY INFORMATION FOR

Biomechanical properties of the jaws of two species of *Clevosaurus* and a reanalysis of the rhynchocephalian dentary morphospace

by SOFIA A.V. CHAMBI-TROWELL¹, DAVID I. WHITESIDE^{1,2}, MICHAEL J. BENTON¹ and EMILY J. RAYFIELD¹

¹ School of Earth Sciences, University of Bristol, Bristol, BS8 1TF, UK;
sc14927@my.bristol.ac.uk, David.Whiteside@bristol.ac.uk, mike.benton@bristol.ac.uk,
e.rayfield@bristol.ac.uk

² Palaeontology Section, Earth Science Department, The Natural History Museum, Cromwell Road, London SW7 5BD, UK

Table of Contents

Sections:

- A. CT-scan parameters
- B. Homologous points on the mandibular ramus of *Clevosaurus* used for figure 6
- C. Morphometrics data
- D. Description of the adductor musculature of *Clevosaurus*
- E. Finite element analyses output (.rpt)
- F. Surface files for left mandibular ramus of *Clevosaurus* (.stl)
- G. Supplementary tables
 - Tables S1–S5

Figures S1–S5

References cited in supplementary information

A. CT-scan parameters:

The cranial material of *Clevosaurus cambrica* (NHMUK PV R37014) was scanned at the University of Bristol, for 2.5 hours, using a Nikon XTH225ST CT Scanner. The scan settings were 224kVp, 117 μ A, 1s exposure, 3141 projections using an average of 2 frames per projection, acquired during a full 360° rotation with source to detector distance of 1176 mm and source to object distance of 152 mm, resulting in a 0.0258 μ m reconstructed voxel resolution. A 0.5-mm Cu filter was used. This material was first used in Keeble *et al.* 2018 but was later reanalysed and processed anew in Chambi-Trowell *et al.* 2019.

Though not used in paper, we also include here the forelimb and pectoral girdle of *C. cambrica* (NHMUK PV R37013), as it belongs to the same animal as NHMUK PV R37014. NHMUK PV R37014 was scanned at the University of Bristol, for 2.5 hours, using a Nikon XTH225ST CT Scanner. The scan settings were 224kVp, 130 μ A, 1.41s exposure, 3141 projections using an average of 2 frames per projection, acquired during a full 360° rotation with source to detector distance of 1176 mm and source to object distance of 158 mm, resulting in a 0.0269 μ m reconstructed voxel resolution. A 1.5-mm Cu filter was used. This material was first used in Keeble *et al.* 2018, but was later reanalysed and processed anew in Chambi-Trowell *et al.* 2019.

The scanning process of the cranial material of *Clevosaurus hudsoni* (NHMUK PV R36832) has been described before in O'Brien *et al.* 2018, but we include it here for the sake of convenience to compliment to the CT-scans available for this skull at the dryad depository.

This material was scanned at the University of Southampton, using a custom built, dual source 225/450 kV walk-in room (Nikon Metrology, UK). The specimen was mounted within a Perspex tube in phenolic foam. The scan settings were 160 kVp, 44 μ A, 177 ms exposure, 3142 projections using an average of 64 frames per projection, acquired during a full 360° rotation with a 702 mm source to detector distance, and a 180 mm source to object distance, resulting in a 51 μ m reconstructed voxel resolution; though this was adjusted to obtain a 30 μ m reconstructed voxel resolution (further detail not provided; see O'Brien *et al.* 2018)). A 1-mm Cu filter was used, in addition to the beryllium window which forms part of the target housing. The scan was acquired with a microfocus 225 kV source, fitted with a tungsten reflection target and a Perkin Elmer XRD 1621 detector. The scan was reconstructed using CTPro and CTAgent software packages (Nikon Metrology), with a filtered back projection algorithm. The original CT-scan images are both available on request from the Natural History Museum of London.

B. Homologous points on the mandibular ramus of *Clevosaurus* used for figure 6:

(1) the base of the retroarticular process, (2) across the articular condyle, (3) anterior of the articular condyle, (4) midway between the highest point of the coronoid process and the articular condyle, (5) the highest point of coronoid process, (6) the lowest point of “diastema” anterior to the coronoid process, (7) across the ultimate tooth at its highest point, (8) dentary immediately anterior of ultimate tooth, (9) across the penultimate tooth at its highest point, (10) dentary immediately anterior of penultimate tooth, (11) across the anterior-most tooth at its highest point, (12) dentary immediately anterior of ultimate tooth.

C. Morphometrics data

An excel file containing the list of landmarks used, specimen numbers, Procrustes distances results and groupings (e.g. cladistic, period, continent).

D. Description of the adductor musculature of *Clevosaurus*

M. adductor mandibulae externus superficialis (mAMES) In *C. hudsoni*X, this muscle originates from the medial surface of the supratemporal bar formed by the postorbital and

squamosal. This is inferred by a concavity on the medial surface of the postorbital, anteriorly limited by a prominent vertical ridge that forms part of the orbital rim and runs behind the postfrontal facet. Attachment on the medial surface of the squamosal is also indicated by a concave surface. The caudal extent of origin is unclear, and mainly inferred from *Sphenodon* (Jones *et al.* 2009) and limited by the position of the mAMEP. In *Sphenodon*, the mAMES also originates from the fascia of the lower temporal fenestra. In *C. hudsoniX* this is inferred (Fig. 4C), and we assume no part of the origin was on the lower temporal bar, although poor preservation means we cannot test this. We have to further infer that the muscle originated from a similar position in *C. cambrica* as its supratemporal bar is incomplete and poorly preserved.

Insertion takes place on the posterolateral surface of the dentary and coronoid process. In *C. hudsoniX* we place this on the smooth wide surface that extends caudally along the lateral surface of the dentary from close to the anterior point of the coronoid process. A similar site can be inferred in *C. cambrica*. Insertion on the surangular is not certain in *Clevosaurus* but is suggested from *Sphenodon*, as described by Gorniak *et al.* (1982).

M. adductor mandibulae externus medialis (mAMEM) The mAMEM originates from the posteromedial surface of the parietal in *C. hudsoniX* and *C. cambrica*, indicated by a smooth but defined slope that separates it from the dorsal medial side of the parietal. The mAMEM also has a site of origin along the anterior surface of the posterior process of the squamosal (as in *Sphenodon*; Abdala and Moro 2003), which is concave. Its lower vertical extent on the parietal, which is a site of origin shared with the mAMEP, is not clear but inferred through proportions and cross-sections in *Sphenodon* (Jones *et al.* 2009). The anterior extent of the mAMEM is marked by a notch on the medial side of the parietal, while the caudal extent is unclear but is inferred from *Sphenodon* not to extend beyond the parietal process.

In *Sphenodon*, insertion takes place on the lateral surface of the basal aponeurosis of the mandible (Wu 2003), which originates along the dorsal margin of the coronoid and surangular. In *Clevosaurus*, we infer the same position of insertion; there is no osteological evidence in either specimen.

M. adductor mandibulae externus profundus (mAMEP). The mAMEP originates from the posteromedial surface of the parietal, indicated by a smooth slope shared with the mAMEM in both *C. hudsoniX* and *C. cambrica*. The dorsal extent on the parietal is constrained by the position of the mAMEM, and the anterior extent is marked by a notch on the medial side of the parietal. The caudal extent is unclear but inferred to extend to a depression on the anterior surface of the posterior process of the squamosal, and possibly the dorsolateral surface of the quadrate as well, as in *Sphenodon*. Alternatively, some muscle fibres in *Sphenodon* may also originate from the prootic (Haas 1973; Gorniak *et al.* 1982), but this cannot be verified in either *Clevosaurus* species. In any case, because of the way in which the muscles pack into the adductor chamber, this region is already overlain by the mAMEP in our reconstructions.

Insertion occurs on the medial surface of the basal aponeurosis. We refer to *Sphenodon* to estimate the extent of insertion on the dorsal margin of the coronoid process and articular complex.

M. pseudotemporalis profundus (mPstP) originates from the posterolateral edge of the epipterygoid, marked by a smooth flattened surface that is clearly distinct from the anterolateral edge in *C. hudsoniX*, and therefore probably also in *C. cambrica* where this level of detail is not preserved on the epipterygoid. In *Sphenodon* it may also attach to the parietal (Haas, 1973, but see Wu, 2003), but there is no evidence that this was the case in either of our *Clevosaurus* specimens.

The muscle inserts into the medial surface of the coronoid (inferred from *Sphenodon*; Haas 1973; Gorniak *et al.* 1982; Wu 2003). However, its extent is unclear in our specimens, and is confined by the placement of the mPstS which inserts directly above the mPstP. In *Sphenodon*, its extent is from the anterior end of the coronoid process to the anterior medial surface of the articular complex (Haas 1973; Gorniak *et al.* 1982; Wu 2003), and is posteriorly constrained by the mAMEM.

M. pseudotemporalis superficialis (mPstS) In both species of *Clevosaurus*, the mPstS originates from the anterolateral surface of the parietal and runs anteriorly to the posterior edge of the postfrontal, as in *Sphenodon* (Haas 1973). The caudal extent of the site of origin is limited by a notch along the lateral surface of the parietal, indicated by a smooth, sloping, shelf-like step on the dorsolateral edge of the parietal, the same shelf that is shared posteriorly with the mAMEM and mAMEP.

In *Sphenodon* insertion takes place on the medial surface of the basal aponeurosis (Haas 1973). Since this is not preserved in *Clevosaurus*, the region of attachment must be estimated along the posteromedial surface of the coronoid process, placed directly above the mPstP. In *Sphenodon* at least some fibres insert directly on the coronoid (Wu 2003) and this may also be the case in *C. hudsoniX* and *C. cambrica* because of their large coronoids.

M. pterygoideus typicus (mPtTy) originates from the medial surface of the quadrate-ptyergoid flange, confined to the anterodorsal margin of the pterygoid and anteromedial process of the quadrate and medial surface of the ectopterygoid-ptyergoid process, as inferred from *Sphenodon* (Jones *et al.* 2009). The thin bones of the quadrate and pterygoid flanges are preserved in both specimens, but they are of low resolution and sites of muscle origin can only be inferred. In *Sphenodon*, there is a medial pterygoid crest (Gorniak *et al.* 1982) that marks the anterior limit of origin. In *C. hudsoniX*, the pterygoid appears to be broken close to the site of the pterygoid-ectopterygoid process and the palatine is missing, so the medial pterygoid crest is not well defined, if present, but it is clearly visible in *C. cambrica*.

The mPtTy inserts into the postero-medial and ventral surfaces of the dentary. The anterior extent is limited by a prominent ridge running up the ventral portion of the dentary. Jones *et al.* (2009) found that some of the posterior-most muscle fibres also inserted between the articular surface and the mDM in *Sphenodon*, whereas the articular complex and retroarticular in *C. hudsoniX* and *C. cambrica* are large and elongate, providing an extensive surface for muscle insertion. The articular of *C. hudsoniX* has a flattened medial surface, the caudal-most regions of which limit the extent of the mPtTy site of insertion, whereas in *C. cambrica* this is not as well defined but is inferred. In *Sphenodon*, muscle fibres that insert into the articular complex can provide an opposing force during jaw closure, and this might have helped to stabilise the jaw to ensure precise occlusion (Jones *et al.* 2009), as it could have done in *Clevosaurus*. Gorniak *et al.* (1982) found that the mPtTy was the heaviest muscle in *Sphenodon* and could be divided into three parts. Here the muscle is treated as one, and it was the largest cranial muscle in *C. hudsoniX*, as its volume exceeds that of the second largest muscle, the mAMES.

M. pterygoideus atypicus (mPtAt) originates via a tendon from the dorsal surface of the palatine-ptyergoid joint in *Sphenodon* (Jones *et al.* 2009). However, the palatines of our two specimens are of too low resolution for any osteological correlates to be observed. Therefore, the site of origin was inferred from *Sphenodon*, positioned just in front of the palatine-ptyergoid joint, and then folded over the ectopterygoid-ptyergoid joint.

Insertion takes place on the medial surface of the coronoid process (Holliday and Witmer 2007; Jones *et al.* 2009) and is limited dorsally by the mPstP and mPstS. The site of origin on the coronoid process is unclear and is mainly inferred from *Sphenodon* and is confined dorsally by the mPstP. The site of insertion in *Sphenodon* is subject to individual variation (Jones *et al.* 2009), so it is also possible that some muscle fibres were inserted into the lower margin of the adductor fossa as in *Sphenodon* (Wu 2003), but this has not been modelled here. The mPtAt is absent in extant squamates, such as *Uromastyx* and *Tupinambis* (Haas 1973; Wu 2003).

M. adductor mandibulae posterior (mAMP) originates from the lateral surface of the quadrate-ptyergoid process, and therefore the site of origin is deduced from *Sphenodon* as is its insertion into the adductor fossa (Haas 1973; Wu 2003; Holliday & Witmer 2007; Jones *et al.* 2009). The site of origin was mainly confined to the thicker ventral process of the quadrate-ptyergoid flange and is dorsally confined by the extent of the mAMEP. As in *Sphenodon* (Haas 1973; Wu 2003), the muscle fibres were estimated to be oriented at about

90 degrees to the long axes of the jaws during occlusion. The adductor fossa is more clearly defined in *C. cambrica* and is the site of insertion.

M. depressor mandibulae (mDM) is involved in opening the jaws (Gorniak *et al.* 1982). Because we focus on bite force, this muscle is not modelled here. This muscle originates from the posterodorsal surface of the squamosal and parietal process respectively, with the former site marked by some rugosity in *C. hudsoni*X, as in *Sphenodon* (Al-Hassawi 2007), but this region of the squamosal is either damaged or too poorly resolved in *C. cambrica* for this rugosity to be confirmed. Insertion takes place on the retroarticular process, but this is inferred from *Sphenodon*, where it attaches to a tendon that inserts into a very small region of the posterolateral tip of the retroarticular process – in our specimens the fibres are inserted into the ventral surface of the articular and anterior region of the retroarticular process.

E. Finite element analyses output (.rpt)

Output data for *Clevosaurus hudsoni* (E1-E2) and *Clevosaurus cambrica* (E3-E6).

- *Clevosaurus hudsoni*: E1 with a bite position at the posterior-most tooth, E2 with a bite position at the anterior-most tooth.
- *Clevosaurus cambrica* (no surface-area to force scaling): E3 with a bite position at the posterior-most tooth, E4 with a bite position at the anterior-most tooth.
- *Clevosaurus cambrica* (with surface-area to force scaling): E5 with a bite position at the posterior-most tooth, E6 with a bite position at the anterior-most tooth.

F. Surface files for the left mandibular ramus of *Clevosaurus* (.stl)

Raw surface files for the lower left mandibular ramus of *Clevosaurus hudsoni* (F1) and *Clevosaurus cambrica* (F2) after reassembly. Note that since these jaws are surface files only, they do not retain separate label fields for the post-dentary bones and have not yet undergone the repairs that were required before pre-processing in FE was initiated.

G. Supplementary tables:

Excel spreadsheet summarising the following tables (tables S1-S5).

	Mean muscle fibre length (mm)	Mean angle of insertion (Coronal, degrees)	Mean angle of insertion (Sagittal, degrees)	Volume (mm ³)	Contribution to bite force*
mAMES	8.43	6.52	1.60	73.66	26.55-21.29%
mAMEM	10.07	18.82	3.76	68.64	19.68-15.79%
mAMEP	10.65	25.20	2.02	41.44	10.76-8.63%
mAMP	4.11	3.47	5.83	4.84	3.58-2.87%
mPstS	8.10	19.33	2.08	9.83	3.50-2.81%
mPstP	7.32	28.53	5.43	2.83	1.03-0.83%
mPtTy	9.28	4.85	22.74	106.23-187.72*	32.15-45.58%
mPtAt	4.91	31.3	33.03	6.17	2.75-2.21%

Table S1. Calculated muscle values for *Clevosaurus hudsoni*X (NHMUK PV R36832), used in the calculation of bite force and the finite element analysis of the mandible. *C. hudsoni*X = proposed second example of Swinton's *C. hudsoni* morphotype (1939). * = the higher end of the range is based on the alternative mPtTy reconstruction.

	Mean muscle fibre length (mm)	Mean angle of insertion (Coronal, degrees)	Mean angle of insertion (Sagittal, degrees)	Volume (mm ³)	Contribution to bite force*
mAMES	6.00	10.63	4.62	45.27	47.02-31.56%
mAMEM	5.71	38.19	17.40	15.58	13.00-8.72%
mAMEP	7.10	39.54	6.17	12.69	8.72-5.85%
mAMP	4.01	75.70	6.25	11.01	4.28-2.87%
mPstS	5.55	39.79	13.09	6.66	5.71-3.83%
mPstP	5.41	35.00	10.99	0.63	0.60-0.40%
mPtTy	4.58	26.39	39.39	21.32-72.34*	20.49-46.64%
mPtAt	5.21	67.29	81.97	2.03	0.17-0.12%

Table S2. Calculated muscle values for *Clevosaurus cambrica* (NHMUK PV R37014), used in the calculation of bite force and the finite element analysis of the mandible. * = the higher end of the range is based on the alternative mPtTy reconstruction.

	<i>Clevosaurus cambrica</i>		<i>Clevosaurus hudsoniX</i>	
	Ultimate Tooth	Anterior-most Tooth	Ultimate Tooth	Anterior-most Tooth
Maximum von Mises stress (MPa)	58.52	78.71	106.09	86.73
Maximum principal strain (microstrain)	2.13x10 ⁻³	4.07x10 ⁻³	1.21x10 ⁻³	1.56x10 ⁻³
Maximum bite force values (N)	6.70	3.99	12.91	9.14
Mechanical Advantage	0.43	0.26	0.45	0.32
Median von Mises stress (MPa)	5.39	15.25	4.59	5.71
Median principal strain (microstrain)	2.18x10 ⁻⁴	5.38x10 ⁻⁴	1.91x10 ⁻⁴	2.30x10 ⁻⁴

Table S3. Finite Element Analysis output for the mandibles of *Clevosaurus cambrica* (NHMUK PV R37014) and *Clevosaurus hudsoniX* (NHMUK PV R36832) without scaling. *C. hudsoniX* = proposed second example of Swinton's *C. hudsoni* morphotype (1939). maximum von Mises stress and maximum principal strain taken as a 0.995 percentile of output.

	<i>Clevosaurus cambrica</i> (anterior-most)	<i>Clevosaurus cambrica</i> (ultimate)	<i>Clevosaurus hudsoniX</i> (anterior-most)	<i>Clevosaurus hudsoniX</i> (ultimate)
10%	2.26	1.0x10 ⁻⁴	0.17	8.0x10 ⁻³
20%	5.27	0.05	1.80	0.91
25%	6.60	0.46	2.55	1.77
30%	8.07	1.41	3.20	2.40
40%	11.37	3.40	4.40	3.53
50%	15.25	5.39	5.71	4.59
60%	19.42	7.78	7.24	5.80
70%	23.85	11.21	9.11	7.38
75%	26.58	13.32	10.21	7.39
80%	29.9	15.67	11.58	9.55
90%	40.07	23.20	15.85	12.82

Table S4. Percentile values for von Mises stress values for *Clevosaurus hudsoniX* (NHMUK PV R36832) and *Clevosaurus cambrica* without scaling. (NHMUK PV R37014), when the bite point is at the anterior-most tooth and the ultimate tooth. *C. hudsoniX* = proposed second example of Swinton's *C. hudsoni* morphotype (1939).

	<i>Clevosaurus cambrica</i> (anterior-most)	<i>Clevosaurus cambrica</i> (ultimate)	<i>Clevosaurus hudsoniX</i> (anterior-most)	<i>Clevosaurus hudsoniX</i> (ultimate)
10%	4.92	2.5×10^{-4}	0.17	8.0×10^{-3}
20%	11.45	0.11	1.80	0.91
25%	14.36	0.99	2.55	1.77
30%	17.55	3.01	3.20	2.40
40%	24.64	7.40	4.40	3.53
50%	33.18	11.73	5.71	4.59
60%	42.25	16.92	7.24	5.80
70%	51.89	24.39	9.11	7.38
75%	57.82	28.98	10.21	7.39
80%	65.06	34.10	11.58	9.55
90%	87.17	50.47	15.85	12.82

Table S5. Percentile values for von Mises stress values for *Clevosaurus hudsoniX* (NHMUK PV R36832) and *Clevosaurus cambrica*, with surface area to force scaling. (NHMUK PV R37014), when the bite point is at the anterior-most tooth and the ultimate tooth. *C. hudsoniX* = proposed second example of Swinton's *C. hudsoni* morphotype (1939).

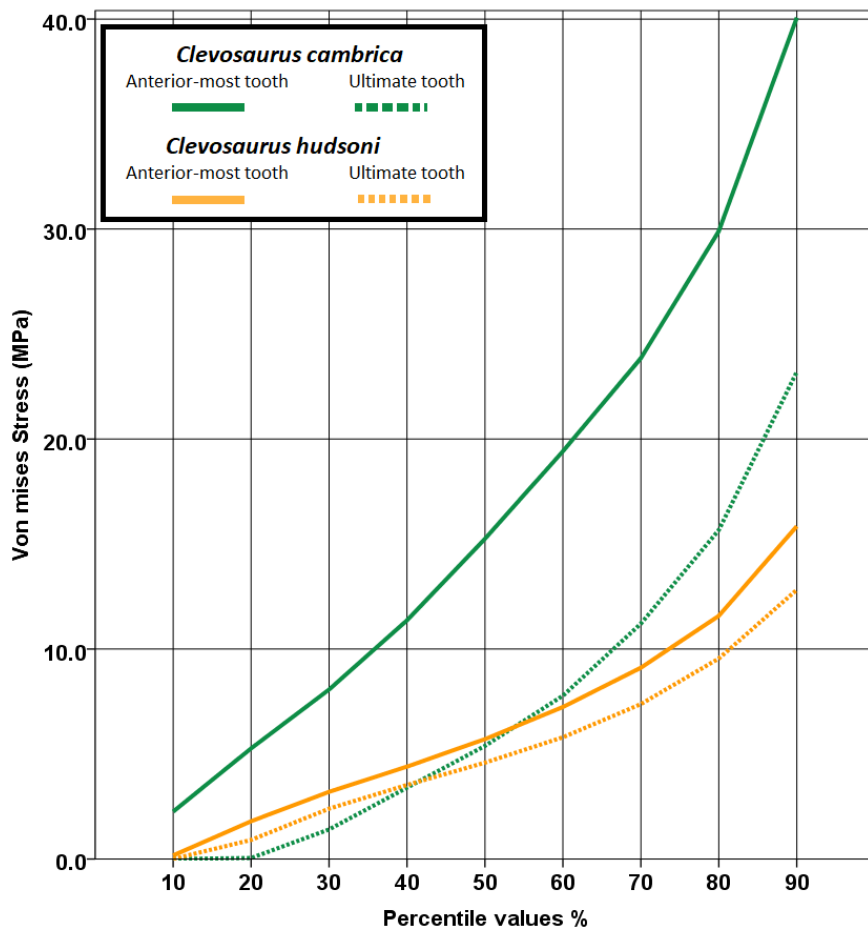


Figure S1. Percentile values for von Mises stress values for *Clevosaurus hudsoni*X (NHMUK PV R36832) and *Clevosaurus cambrica* where surface-area-to-force is not scaled. (NHMUK PV R37014), when the bite point is at the anterior-most tooth and the ultimate tooth. *C. hudsoni*X = proposed second example of Swinton's *C. hudsoni* morphotype (1939).

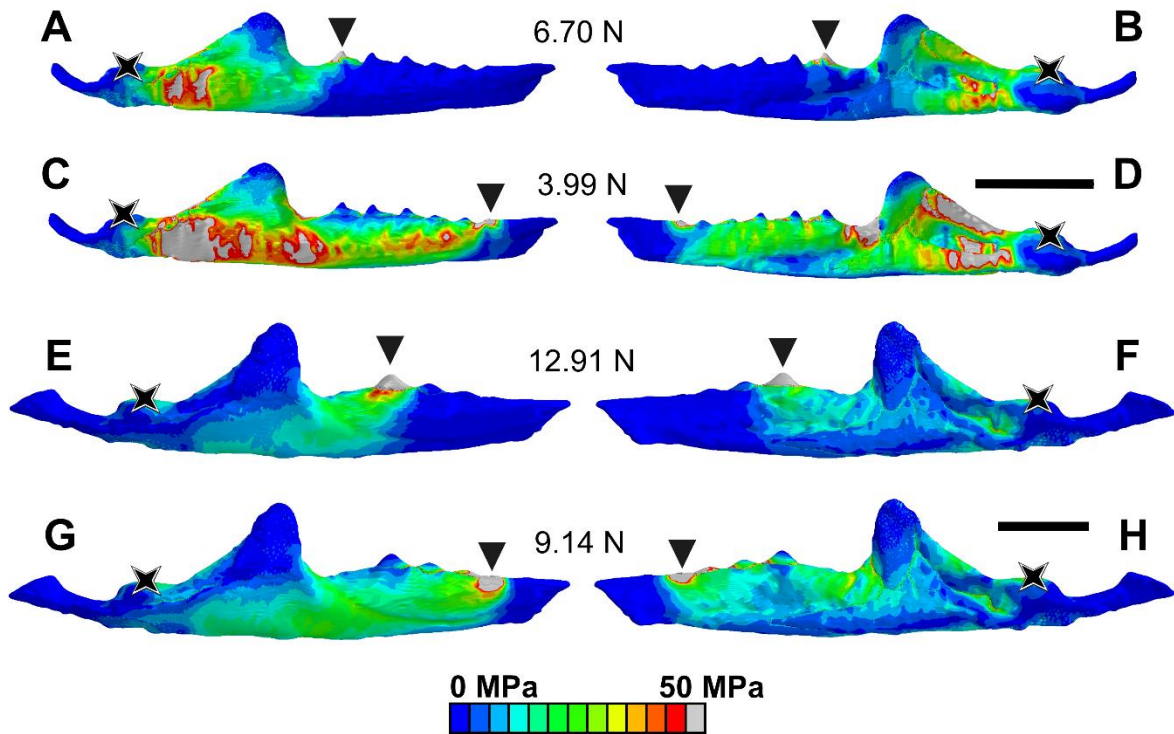


Figure S2. Finite element von Mises stress contour plots for the right mandible of *Clevosaurus cambrica* (NHMUK PV R37014) and mirrored left mandible of *Clevosaurus hudsoniX* (NHMUK PV R36832) with no scaling. For *Clevosaurus cambrica* with a bite point at the ultimate tooth in lateral (A) and medial (B) views, and the anterior-most tooth for in lateral (C) and medial (D) views; and of the mirrored left mandible of *Clevosaurus hudsoniX* for a bite point at the ultimate tooth in lateral (E) and medial (F) views, and for the anterior-most tooth in lateral (G) and medial (H) views. Bite point is indicated with an arrow, while the condyle/fulcrum is indicated by a star. *C. hudsoniX* = proposed second example of Swinton's *C. hudsoni* morphotype (1939).

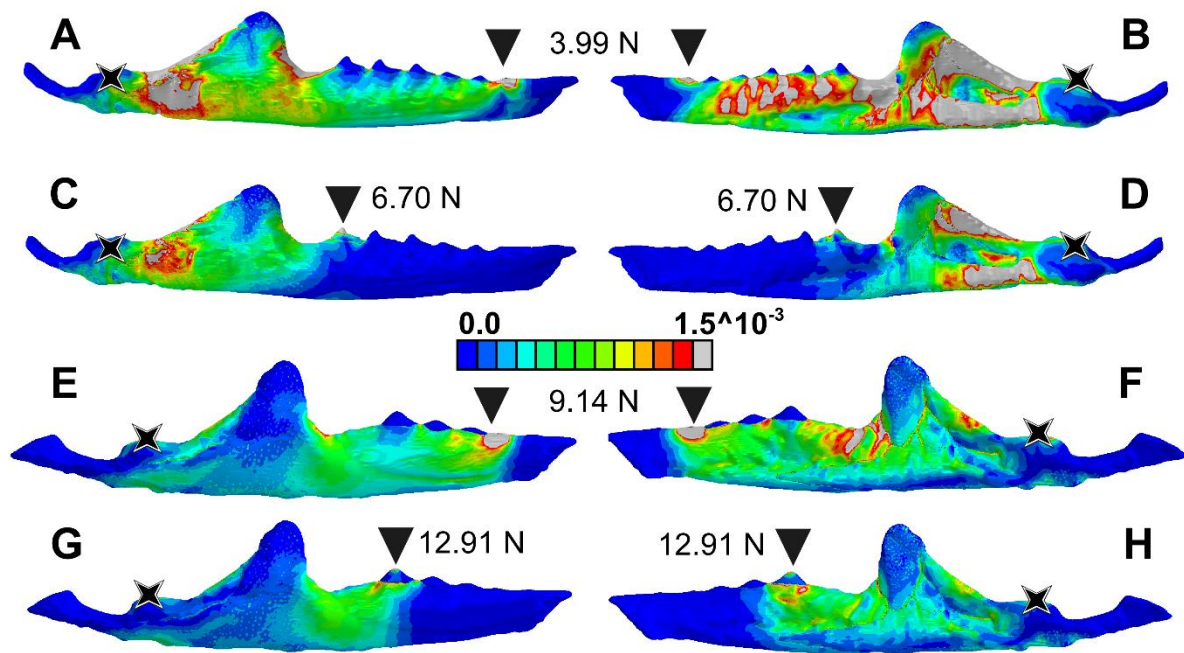


Figure S3. Finite element maximum principal strain contour plots for the right mandible of *Clevosaurus cambrica* (NHMUK PV R37014) and mirrored left mandible of *Clevosaurus hudsoniX* (NHMUK PV R36832) with no scaling. For *Clevosaurus cambrica* with a bite point at the anterior-most tooth in lateral (A) and medial (B) views, and for the ultimate tooth in lateral (C) and medial (D) views; and of the mirrored left mandible of *Clevosaurus hudsoniX* for a bite point at the anterior-most tooth in lateral (E) and medial (F) views, and for the ultimate tooth in lateral (G) and medial (H) views. Bite point is indicated with an arrow, while the condyle/fulcrum is indicated by a star. *C. hudsoniX* = proposed second example of Swinton's *C. hudsoni* morphotype (1939).

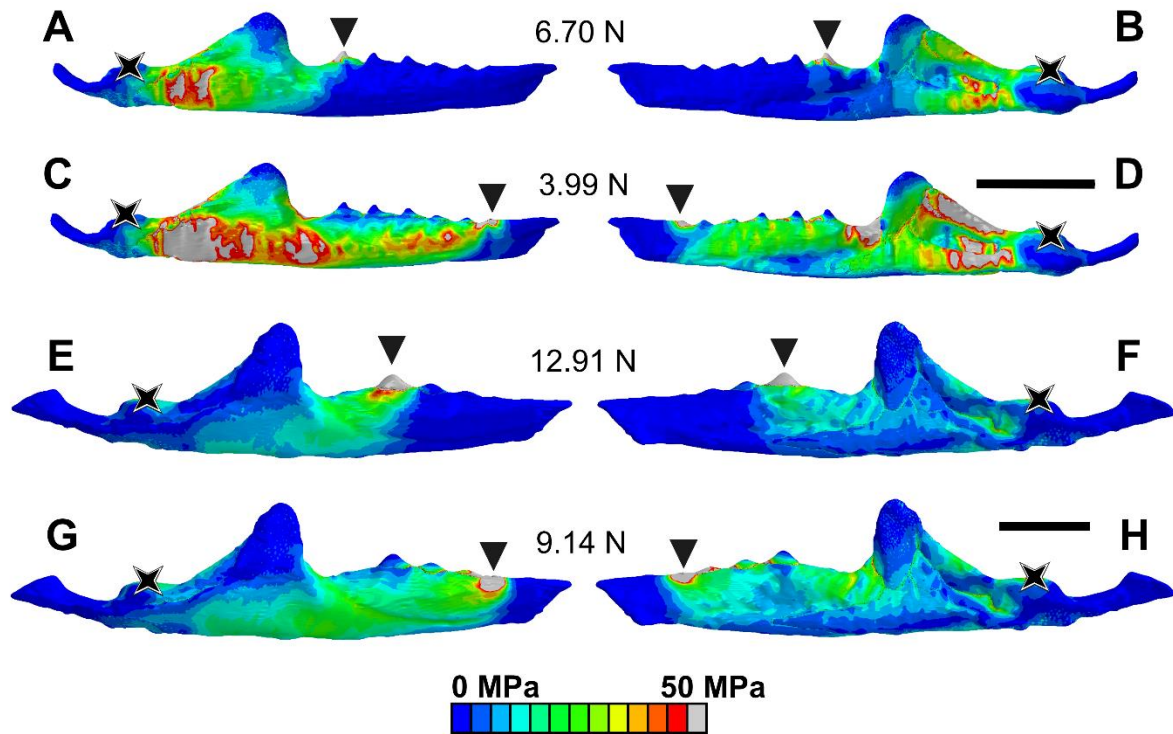


Figure S4. Finite element von Mises stress contour plots for the right mandible of *Clevosaurus cambrica* (NHMUK PV R37014) and mirrored left mandible of *Clevosaurus hudsoniX* (NHMUK PV R36832) with surface-area-to-force scaling. For *Clevosaurus cambrica* with a bite point at the ultimate tooth in lateral (A) and medial (B) views, and for the anterior-most tooth in lateral (C) and medial (D) views; and of the mirrored left mandible of *Clevosaurus hudsoniX* for a bite point at the ultimate tooth in lateral (E) and medial (F) views, and for the anterior-most tooth in lateral (G) and medial (H) views. Bite point is indicated with an arrow, while the condyle/fulcrum is indicated by a star. *C. hudsoniX* = proposed second example of Swinton's *C. hudsoni* morphotype (1939).

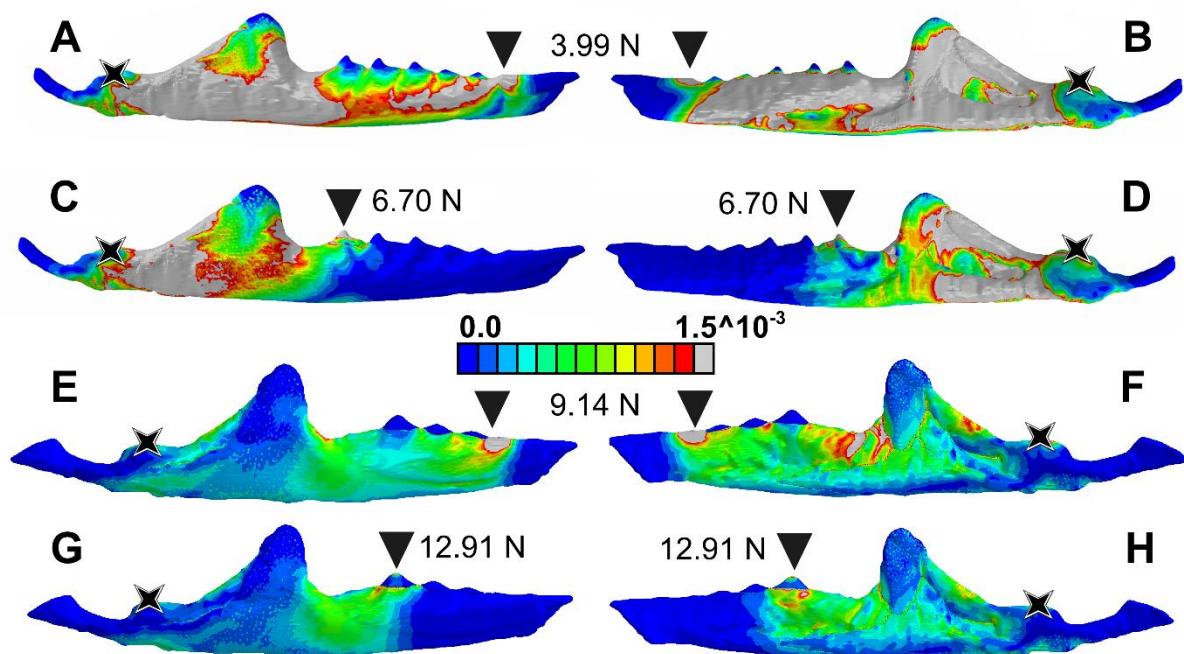


Figure S5. Finite element maximum principal strain contour plots for the right mandible of *Clevosaurus cambrica* (NHMUK PV R37014) and mirrored left mandible of *Clevosaurus hudsoniX* (NHMUK PV R36832) with surface-area-to-force scaling. For *Clevosaurus cambrica* with a bite point at the anterior-most tooth in lateral (A) and medial (B) views, and for the ultimate tooth in lateral (C) and medial (D) views; and of the mirrored left mandible of *Clevosaurus hudsoniX* for a bite point at the anterior-most tooth in lateral (E) and medial (F) views, and for the ultimate tooth in lateral (G) and medial (H) views. Bite point is indicated with an arrow, while the condyle/fulcrum is indicated by a star. *C. hudsoniX* = proposed second example of Swinton's *C. hudsoni* morphotype (1939).

References

- CHAMBI-TROWELL, S. A. V., WHITESIDE, D. I. and BENTON, M. J. 2019. Diversity in rhynchocephalian *Clevosaurus* skulls based on CT reconstruction of two Late Triassic species from Great Britain. *Acta Palaeontologica Polonica*, **64**, 41–64.
- KEEBLE, E., WHITESIDE, D. I. and BENTON, M. J. 2018. The terrestrial fauna of the Late Triassic Pant-y-ffynnon Quarry fissures, South Wales, UK and a new species of *Clevosaurus* (Lepidosauria: Rhynchocephalia). *Proceedings of the Geologists' Association*, **129**, 99–119.
- O'BRIEN, A., WHITESIDE, D. I. and MARSHALL, J. E. A. 2018. Anatomical study of two previously undescribed specimens of *Clevosaurus hudsoni* (Lepidosauria: Rhynchocephalia) from Cromhall Quarry, UK, aided by computed tomography, yields additional information on the skeleton and hitherto undescribed bones. *Zoological Journal of the Linnean Society*, **183**, 163–195.